PHYSICAL REVIEW D **70,** 116006 (2004)

Collective modes of an anisotropic quark-gluon plasma: II

Paul Romatschke and Michael Strickland

Institut für Theoretische Physik, Technische Universität Wien, Wiedner Hauptstrasse 8-10, A-1040 Vienna, Austria

(Received 8 July 2004; published 6 December 2004)

We continue our exploration of the collective modes of an anisotropic quark-gluon plasma by extending our previous analysis to arbitrary Riemann sheets. We demonstrate that in the presence of momentum-space anisotropies in the parton distribution functions there are new relevant singularities on the neighboring unphysical sheets. We then show that for sufficiently strong anisotropies that these singularities move into the region of spacelike momentum and their effect can extend down to the physical sheet. In order to demonstrate this explicitly we consider the polarization tensor for gluons propagating parallel to the anisotropy direction. We derive analytic expressions for the gluon structure functions in this case and then analytically continue them to unphysical Riemann sheets. Using the resulting analytic continuations we numerically determine the position of the unphysical singularities. We then show that in the limit of infinite contraction of the distribution function along the anisotropy direction that the unphysical singularities move onto the physical sheet and result in real spacelike modes at large momenta for all "out-of-plane" angles of propagation.

DOI: 10.1103/PhysRevD.70.116006 PACS numbers: 11.15.Bt, 04.25.Nx, 11.10.Wx, 12.38.Mh

I. INTRODUCTION

The ultrarelativistic heavy ion collision experiments ongoing at the Brookhaven Relativistic Heavy Ion Collider (RHIC) and planned at the CERN Large Hadron Collider study the behavior of nuclear matter under extreme conditions. Specifically, these experiments explore the QCD phase diagram at large temperatures and small quark chemical potentials. Based on the data currently available from the RHIC collisions it seems that a thermalized state has been created during the collisions [1]. Remarkably it seems that the thermalization proceeds rather rapidly in contradiction to estimates from leading order equilibrium perturbation theory. However, to truly understand how the plasma evolves and thermalizes one has to go beyond the equilibrium description. In this paper we expand upon our previous studies of the collective modes of a quark-gluon plasma which is (at least approximately) homogeneous and stationary but anisotropic in momentum space.

These types of distribution functions are relevant because of the approximate longitudinal boost invariance in the central rapidity region of ultrarelativistic heavy ion collisions. This implies that the initial distribution functions for the partons are practically delta functions in longitudinal momentum. Such an anisotropic quark-gluon plasma appears to be qualitatively different from the isotropic one since the quasiparticle collective modes can then be unstable [2–10]. The presence of these instabilities can dramatically influence the system's evolution leading, in particular, to its faster equilibration and isotropization. Treating this problem in all of its generality is a daunting task. In order to make progress we consider the limit of very high transverse temperatures at which the nonequilibrium collective behavior is describable in terms of processes in which all loop momenta are *hard*. In the case of thermal equilibrium hard corresponds to momenta of order T but in the nonequilibrium case hard corresponds to an unspecified scale contained in the distribution function.

In a previous paper [7] we calculated the hard-loop gluon polarization tensor in the case that the momentum-space anisotropy is obtained from an isotropic distribution by the rescaling of one direction in momentum space. The resulting expression for the gluon polarization tensor was then decomposed into a four-component tensor basis and the structure functions associated with this tensor basis were computed numerically for general anisotropies and analytically in the limit of small anisotropies. We demonstrated that a contraction of an isotropic distribution function along the anisotropy direction, $\hat{\mathbf{n}}$, resulted in one additional stable quasiparticle mode, two damped quasiparticle modes in the lower half plane, and two unstable (antidamped) quasiparticle modes in the upper half plane. In the case that the isotropic distribution was stretched along the anisotropy direction we found that again an additional stable quasiparticle mode was generated but only one damped and one antidamped quasiparticle mode were found in this case. The unstable modes found correspond to electric or magnetic type instabilities with the latter being analogous to the Weibel instability in QED plasmas [11–15].

In this paper we continue our exploration of the collective modes of an anisotropic quark-gluon plasma by extending our previous analysis to arbitrary Riemann sheets. We demonstrate that in the presence of momentum-space anisotropies in the parton distribution functions there are new relevant singularities on the neighboring unphysical sheets. We then show that for sufficiently strong anisotropies that these singularities move into the region of spacelike momentum and their effect can extend down to the physical sheet. In order to

demonstrate this explicitly we consider the polarization tensor for gluons propagating parallel to the anisotropy direction. We derive analytic expressions for the gluon structure functions in this case and then analytically continue them to unphysical Riemann sheets. Using the resulting analytic continuations we numerically determine the position of the unphysical singularities. We then show that in the limit of infinite contraction of the distribution function along the anisotropy direction that the unphysical singularities move onto the physical sheet and result in real spacelike modes at large momenta for all "out-of-plane" angles of propagation.

The organization of the paper is as follows: In Sec. II we first review the necessary integral expressions for the hard-loop gluon polarization tensor and then in Sec. III we present analytic expressions for the hard-loop gluon polarization tensor structure functions in the case that the gluon is propagating parallel to the anisotropy direction. In Secs. III A, III B, III C, and III D we extend these expressions to arbitrary Riemann sheets and solve the dispersion relations for the singularities existing on the neighboring unphysical sheets. In Sec. IV we present analytic expressions for the gluon polarization tensor structure functions in the large-anisotropy limit and solve the resulting dispersion relations for arbitrary angle of propagation. In Sec. V we summarize the results and speculate about the possible impact of the now relevant unphysical singularities.

II. GLUON POLARIZATION TENSOR REVISITED

The hard-loop gluon polarization tensor of an anisotropic system is given by [4,7]

$$\Pi^{ij}(K) = -2\pi\alpha_s \int \frac{d^3p}{(2\pi)^3} v^i \partial^l f(\mathbf{p}) \left(\delta^{jl} + \frac{v^j k^l}{K\cdot V + i\epsilon} \right), \tag{1}$$

where $K = (\omega, \mathbf{k})$, $V = (1, \mathbf{v})$, $\mathbf{v} = \mathbf{p}/|\mathbf{p}|$, and

$$f(\mathbf{p}) \equiv 2N_f(n(\mathbf{p}) + \bar{n}(\mathbf{p})) + 4N_c n_g(\mathbf{p}). \tag{2}$$

Note that in (1) we have specialized to spacelike Lorentz indices; however, it is possible to derive the polarization tensor also for arbitrary Lorentz indices.

To simplify the calculation we follow Ref. [7] and require the distribution function $f(\mathbf{p})$ to be given by

$$f(\mathbf{p}) = f_\xi(\mathbf{p}) = N(\xi) f_{\rm iso}\left(\sqrt{\mathbf{p}^2 + \xi(\mathbf{p}\cdot\hat{\mathbf{n}})^2}\right). \tag{3}$$

Here $f_{\rm iso}$ is an arbitrary isotropic distribution function, $\hat{\mathbf{n}}$ is the direction of the anisotropy, $\xi > -1$ is a parameter reflecting the strength of the anisotropy, and $N(\xi)$ is a normalization constant. To fix $N(\xi)$ we require that the number density to be the same both for isotropic and arbitrary anisotropic systems,

$$\int_{\mathbf{p}} f_{\rm iso}(p) = \int_{\mathbf{p}} f_\xi(\mathbf{p}) = N(\xi) \int_{\mathbf{p}} f_{\rm iso}\left(\sqrt{\mathbf{p}^2 + \xi(\mathbf{p}\cdot\hat{\mathbf{n}})^2}\right), \tag{4}$$

and can be evaluated to be

$$N(\xi) = \sqrt{1+\xi}. \tag{5}$$

Using an appropriate tensor basis [7] one can then decompose the self-energy into four structure functions α, β, γ, and δ by taking the contractions

$$\begin{aligned} &k^i \Pi^{ij} k^j = k^2 \beta, \qquad \tilde{n}^i \Pi^{ij} k^j = \tilde{n}^2 k^2 \delta, \\ &\tilde{n}^i \Pi^{ij} \tilde{n}^j = \tilde{n}^2(\alpha+\gamma), \qquad {\rm Tr}\Pi^{ij} = 2\alpha + \beta + \gamma, \end{aligned} \tag{6}$$

where $\tilde{n}^i = (\delta^{ij} - k^i k^j/k^2)\hat{n}^j$. The structure functions then depend on ω, k and the angle $\hat{\mathbf{k}}\cdot\hat{\mathbf{n}} = \cos\theta_n$ as well as on the strength of the anisotropy, ξ. Integral expressions for α, β, γ, and δ for arbitrary angle of propagation and anisotropy parameter ξ can be found in Ref. [7].[1]

III. SPECIAL CASE I: $\mathbf{k} \parallel \hat{\mathbf{n}}$

Let us now consider the case where the momentum $\mathbf{k}$ is in the direction of the anisotropy, $\hat{\mathbf{n}}$, i.e., $\theta_n = 0$. Using the changes of variables

$$\tilde{p}^{\,2} = p^2[1 + \xi(\mathbf{v}\cdot\hat{\mathbf{n}})^2], \tag{7}$$

allows us to simplify Eq. (1) to

$$\Pi^{ij}(K) = m_D^2\sqrt{1+\xi} \int \frac{d\Omega}{4\pi} v^i \frac{v^l + \xi(\mathbf{v}.\hat{\mathbf{n}})\hat{n}^l}{[1+\xi(\mathbf{v}.\hat{\mathbf{n}})^2]^2} \times \left(\delta^{jl} + \frac{v^j k^l}{K\cdot V + i\epsilon} \right), \tag{8}$$

where

$$m_D^2 = -\frac{\alpha_s}{\pi} \int_0^\infty dp p^2 \frac{df_{\rm iso}(p^2)}{dp}. \tag{9}$$

Taking the contractions in Eq. (6) the structure functions can further be simplified using

$$\mathbf{k}\cdot\mathbf{v} = k\,\hat{\mathbf{n}}\cdot\mathbf{v} = k\cos\theta. \tag{10}$$

While one integration becomes straightforward, the remaining integration can be performed after a little bit of algebra and one obtains for the relevant contractions

[1] In Ref. [7] $N(\xi)$ was fixed to be $N(\xi) = 1$ so the reader should make sure to adjust for the difference where appropriate.

$$\frac{\alpha}{m_D^2} = \frac{\sqrt{1+\xi}}{4\sqrt{\xi}(1+\xi z^2)^2}\Big[\{1+z^2+\xi[-1+(6+\xi)z^2-(1-\xi)z^4]\}\arctan\sqrt{\xi}+\sqrt{\xi}(z^2-1)$$
$$\times\Big(1+\xi z^2-(1+\xi)z\ln\frac{z+1+i\epsilon}{z-1+i\epsilon}\Big)\Big],$$
$$\frac{\beta}{m_D^2} = -\frac{z^2\sqrt{1+\xi}}{2\sqrt{\xi}(1+\xi z^2)^2}\Big[(1+\xi)(1-\xi z^2)\arctan\sqrt{\xi}+\sqrt{\xi}\Big((1+\xi z^2)-(1+\xi)z\ln\frac{z+1+i\epsilon}{z-1+i\epsilon}\Big)\Big], \tag{11}$$
$$\frac{\hat{\delta}}{m_D^2} = \frac{z\sqrt{1+\xi}}{4\sqrt{\xi}(1+\xi z^2)^3}\Big[z\{-1+\xi[3+6\xi-2(3+6\xi+\xi^2)z^2+\xi(3+\xi)z^4]\}\arctan\sqrt{\xi}$$
$$+\sqrt{\xi}\Big(z(1+\xi z^2)(1+4\xi-3\xi z^2)+\xi(-1+z^2)(-1+4z^2+3\xi z^2)\ln\frac{z+1+i\epsilon}{z-1+i\epsilon}\Big)\Big],$$

where $z=\omega/k$ and $\hat{\delta}=\delta k$. Note that for this angle of propagation the structure function γ vanishes.

A. Extension to unphysical sheets

The above structure functions all possess a logarithmic cut running along the real z axis for $z^2<1$. It is, however, possible to extend their definition beyond this cut, which then corresponds to an unphysical Riemann sheet of z. More precisely, there are two such unphysical sheets which can be accessed by either extending the physical sheet from above or below the cut. In order to make this extension we first compute the structure functions on the physical sheet using the integral representation given in Eq. (8). We can then deform the integration contour which runs from $\cos\theta=-1$ along the real axis to $\cos\theta=1$ into the lower half plane (LHP) and then move the point we are interested in from the upper to the lower half plane. Deforming the original contour so that it again runs along the real axis we see that we pick up an extra contribution corresponding to the residue at the point in the LHP.

This procedure can be used to analytically continue the structure functions for all values of θ_n but in the case that $\theta_n=0$ the residue can be evaluated straightforwardly and is simply $-2\pi i$. The structure functions can likewise be extended into the upper half plane (UHP) and the residue is then $+2\pi i$. The resulting rule is then the expected one, namely, that the structure functions can be extended to unphysical sheets by the usual extension of the logarithm

$$\ln\Big(\frac{z+1}{z-1}\Big)=\ln\Big(\Big|\frac{z+1}{z-1}\Big|\Big)+i\Big[\arg\Big(\frac{z+1}{z-1}\Big)+2\pi n\Big], \tag{12}$$

where n specifies the sheet number. Note that $n=1$ extends the physical logarithm into the UHP and $n=-1$ extends it into the LHP. Higher n correspond to higher sheets which can be safely ignored as we will discuss below.

B. Collective modes

The dispersion relations for the gluonic modes in an anisotropic quark-gluon plasma are in general given by the zeros of

$$\Delta_A^{-1}=k^2-\omega^2+\alpha=0,$$
$$\Delta_G^{-1}=(k^2-\omega^2+\alpha+\gamma)(\beta-\omega^2)-k^2\tilde{n}^2\delta^2=0. \tag{13}$$

In the case $\mathbf{k}\parallel\hat{\mathbf{n}}$, however, γ vanishes identically, as does $\tilde{n}^2=1-(\hat{\mathbf{k}}\cdot\hat{\mathbf{n}})^2$. Therefore, it is sufficient to solve the equations

$$k^2-\omega^2+\alpha=0, \qquad \beta-\omega^2=0, \tag{14}$$

which will be referred to as α and β modes, respectively. These modes correspond to poles in the propagator for α and β modes. We will use this term to describe solutions on both physical and unphysical Riemann sheets; however, whenever we are speaking about the unphysical singularities we will always explicitly label them as *unphysical* α and β modes. The reader should be aware that these unphysical singularities do not correspond to real degrees of freedom unless the solution associated with them moves onto the physical Riemann sheet.

Before we present the dispersion relations we would like to first count the number of modes on the various sheets in order to be assured that we have indeed found all solutions. The number of modes can be counted by doing a so-called Nyquist analysis, based on the special case of Cauchy's integral,

$$N-P=\frac{1}{2\pi i}\oint_C dz\frac{f'(z)}{f(z)}, \tag{15}$$

where N and P are the number of zeros and poles of $f(z)$ times their multiplicity in the region encircled by the closed path C.

Choosing $f(z)=k^2(1-z^2)+\alpha(z)$ and using the explicit form of the structure function given in Eq. (11), one finds that $f(z)$ has a logarithmic cut for real $z^2<1$, while being analytic for all other finite z. One can then choose the contour C depicted in Fig. 1, so that $P=0$. We then

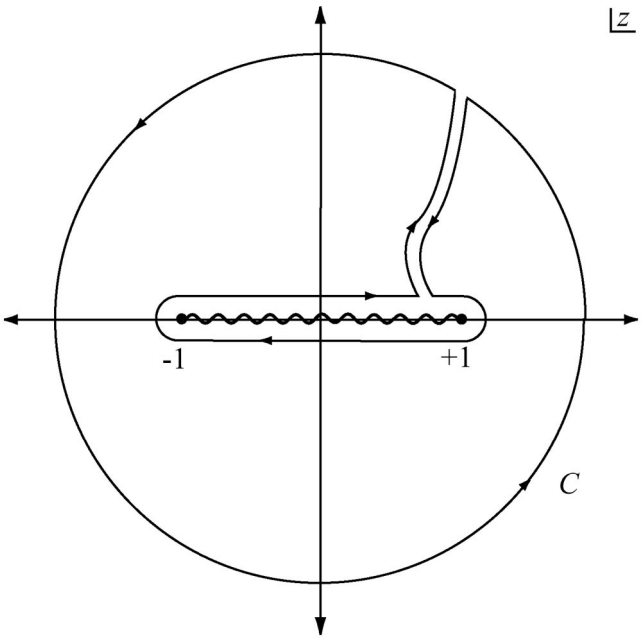

FIG. 1. Contour C in the complex z plane used for finite ξ Nyquist analysis.

evaluate the respective pieces of the contour C, finding

$$N_{\alpha,\mathrm{phys}} = \frac{1}{2\pi i}[4\pi i + 0 + 0 + 4\pi i\Theta(-\lim_{z\to 0} f(z))] = 2 + 2\Theta(-\lim_{z\to 0} f(z)). \quad (16)$$

The first contribution comes from the large circle at $|z| \gg 1$, while the first zero is the contribution from the path connecting the large circle with the contour around $z^2 < 1$; the second zero is the contribution from the small half-circles around $z = \pm 1$. The last contribution comes from the straight lines running infinitesimally above and below the cut at $z^2 < 1$. They can be evaluated by using

$$\int_{-1+i\epsilon}^{1+i\epsilon} dz \frac{f'(z)}{f(z)} = \ln\frac{f(1+i\epsilon)}{f(-1+i\epsilon)}, \quad (17)$$

and therefore represent the "winding number" of the image of $f(z)$ around the origin. Since from Eq. (11) it is clear that $\mathrm{Re}f(-1+i\epsilon) > 0$ and for $z^2 < 1$ one has $\mathrm{Im}f(z) = 0$ only for $z = 0$, the winding number can either be zero or 1, depending on the sign of $\lim_{z\to 0}\mathrm{Re}f(z+i\epsilon)$. For the path with $\mathrm{Im}z < 0$ one proceeds similarly, finding the result given in Eq. (16).

For the β mode, the same techniques can be applied to find the result

$$N_{\beta,\mathrm{phys}} = 2. \quad (18)$$

These two modes, together with two modes coming from $N_{\alpha,\mathrm{phys}}$, correspond to the propagating and stable modes for positive and negative (real) frequencies, while the modes that depend on the sign of the static limit of $f(z)$ correspond to solutions with purely imaginary z which are the damped and antidamped physical modes already found in Ref. [7].

We now want to extend the above analysis to the unphysical sheets that can be accessed by extending the structure functions through the cut to the LHP and UHP, as discussed above. Let us first discuss the α mode in the unphysical LHP by introducing $f_{\mathrm{LHP}}(z) = k^2(1-z^2) + \alpha_{\mathrm{LHP}}(z)$ and choosing a contour C_{LHP} which is shown in Fig. 2. One notable difference to the physical sheet is that now $f_{\mathrm{LHP}}(z)$ has a pole of second order at $z = -i/\sqrt{\xi}$, so that $P_{\alpha,\mathrm{LHP}} = 2$. Other than that the analysis is conducted as in the case above, finding

$$N_{\alpha,\mathrm{LHP}} - P_{\alpha,\mathrm{LHP}} = -\Theta(-\lim_{z\to 0} f_{\mathrm{LHP}}(z)), \quad (19)$$

so that $N_{\alpha,\mathrm{LHP}} = 1 + \Theta(\lim_{z\to 0} f_{\mathrm{LHP}}(z))$.

For the UHP, one uses a similar analysis to find

$$N_{\alpha,\mathrm{UHP}} = 1 + \Theta(\lim_{z\to 0} f_{\mathrm{UHP}}(z)), \quad (20)$$

while for the unphysical β mode one has $N_{\beta,\mathrm{LHP}} = N_{\beta,\mathrm{UHP}} = 2$. Closer inspection of these modes shows that the unphysical α modes correspond to solutions with purely imaginary z, while the unphysical β modes are solutions with complex z with positive/negative real and imaginary parts.

A plot of the position of the unphysical α modes for $\xi = \{0.1, 1, 10\}$ is shown in Fig. 3. Since there are two unphysical α modes we will refer to the ones that depend on the sign of f_{LHP} as type 1 and those which do not as type 2. We can observe from this figure that, as ξ goes to

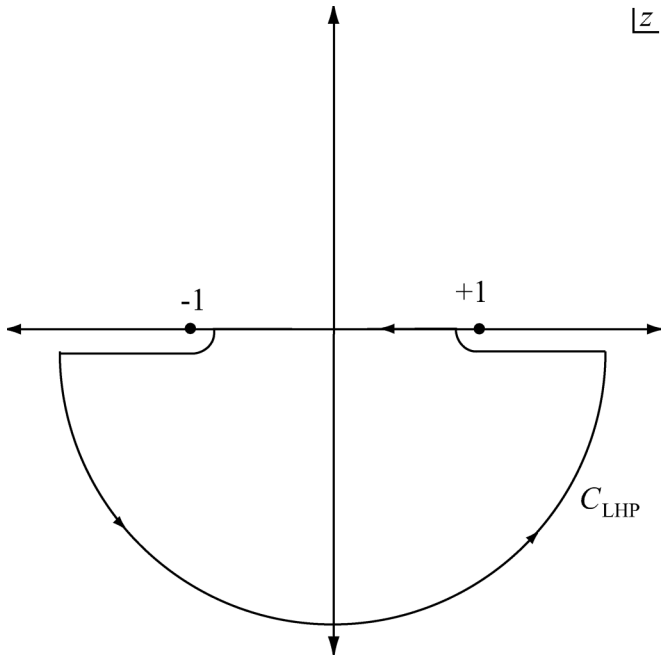

FIG. 2. Contour C_{LHP} in the complex z plane used for finite ξ Nyquist analysis on the LHP unphysical sheet.

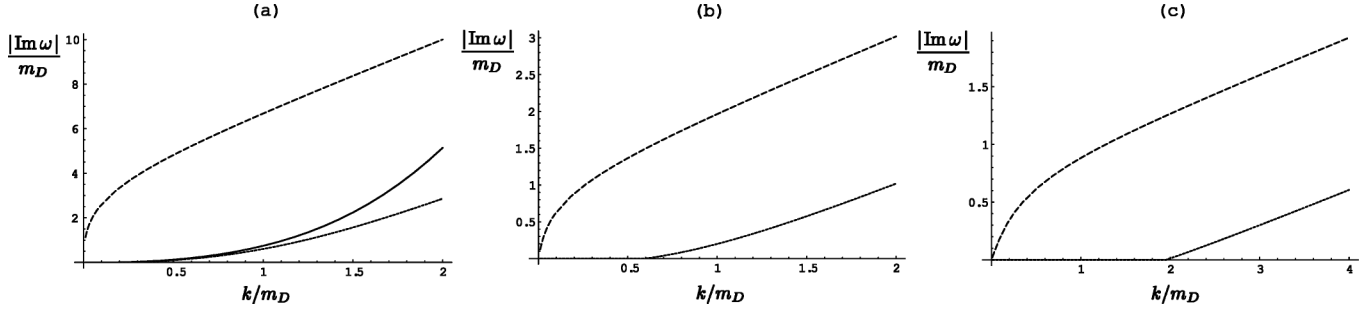

FIG. 3. Dispersion relations for the unphysical α modes for $\theta_n = 0$ and (a) $\xi = 0.1$, (b) $\xi = 1$, and (c) $\xi = 10$. Dotted lines correspond to the modes which depend on the sign of f_{LHP} (type 1). Note that in (a)–(c) the type-1 unphysical α mode exists only for $k > 0.184$, $k > 0.595$, and $k > 1.95$, respectively. Dashed lines correspond to modes which do not depend on the sign of f_{LHP} (type 2). Solid line in (a) is the isotropic result. Note that the scale changes in each plot.

zero, the type-1 mode (dotted line) becomes degenerate with the isotropic solution [solid line in Fig. 3(a)] and the type-2 mode (dashed line) moves off to infinity. In the opposite limit, $\xi \gg 1$, we find that the type-2 mode moves towards the real axis while the threshold for existence of the type-1 mode moves to infinity.

Note that even in the isotropic limit there are unphysical α modes on the neighboring Riemann sheets: one in the UHP and one in the LHP. These unphysical modes are related to the presence of dynamical screening of the magnetic interaction. In fact, in the limit of small momentum it can be shown that these solutions are directly related to the small z behavior of the isotropic transverse polarization tensor. This can be seen by taking the small z and ξ limits of α_{UHP}

$$\lim_{z\to 0}\lim_{\xi\to 0}\frac{\alpha_{\mathrm{UHP}}}{m_D^2} = \frac{iz\pi}{4}\left(1+\frac{3}{8}\xi\right) - \frac{1}{3}\xi + \mathcal{O}(\xi^2, z^2). \quad (21)$$

The first term in (21) comes directly from the logarithmic cut. Taking the isotropic limit, $\xi = 0$, inserting this into the α-mode equation given in Eq. (14), and then taking the static limit we see that there is a solution at purely imaginary ω

$$\omega = \frac{4i}{\pi}\frac{k^3}{m_D^2} + \mathcal{O}(\xi, z^2). \quad (22)$$

Note, however, that the second term in Eq. (21) indicates the presence of unstable modes on the physical sheet for this angle of propagation and, as a result, the isotropic and anisotropic dispersion relations for the unphysical α modes are not trivially connected. This is demonstrated by the fact that the type-1 mode (dotted lines) in Fig. 3 do not extend down to $k = 0$ for finite ξ but instead terminate at a finite $k = k_0$. Below k_0 the type-1 mode in the LHP moves onto the physical sheet and becomes the unstable (antidamped) physical α mode already discussed in Ref. [7]. The type-1 mode in the UHP likewise moves onto the physical sheet and becomes the damped physical α-mode solution.

A plot of the dispersion relations of the physical and unphysical β modes for $\xi = 10$ is shown in Fig. 4 (the mirror region $\mathrm{Re}z < 0$ is not shown). As one can see, the unphysical $\beta_{\mathrm{LHP/UHP}}$ mode is lightlike for small momentum and spacelike at large momentum. As we will discuss below this mode is physically relevant if $\mathrm{Re}z$ is approximately spacelike, $(\mathrm{Re}z)^2 \lesssim 1$, and the modulus of $\mathrm{Im}z$ is small. In addition, in Fig. 5 we have plotted the position of the unphysical β-mode pole for momentum $k = \{m_D/2, m_D, 2m_D\}$ in the complex plane for various values of ξ.

From Fig. 5 we see that, as the anisotropy is decreased the $\mathrm{Im}z$ of the unphysical β mode becomes large at all momenta and therefore these unphysical modes will have a negligible impact on the propagator on the physical Riemann sheet. However, as the anisotropy is increased with fixed momentum, the modulus of $\mathrm{Im}z$ decreases so that these modes can become relevant for large anisotropies. From Fig. 5 we can also see that for fixed ξ and decreasing k that the unphysical β modes move to $z = \infty$

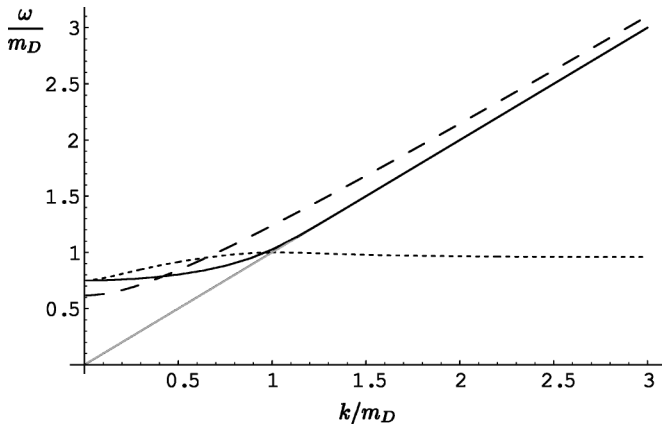

FIG. 4. Dispersion relations for $\theta_n = 0$, $\xi = 10$: besides two propagating α and β modes on the physical sheet (dashed and full lines, respectively) there is also an unphysical β mode (dotted line) for which we plot only the real part of the pole position. We also plot the light cone as a light-gray line as a visual aid.

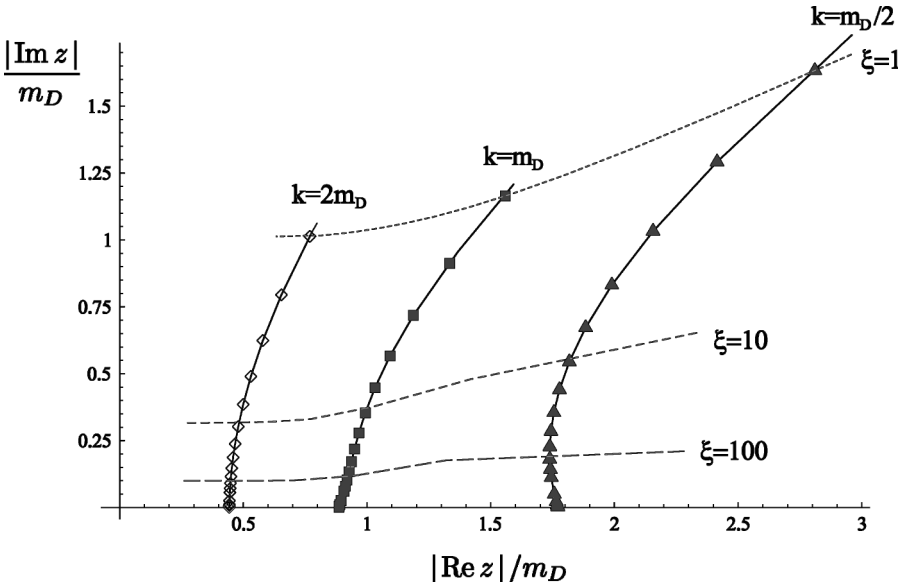

FIG. 5. Parametric plot of the position of the unphysical β mode in the complex z plane for momentum $k = \{m_D/2, m_D, 2m_D\}$ showing that for $k > \sim m_D$ the unphysical β mode moves into the spacelike region of the real z axis for large ξ.

and so are unimportant based on the criteria stated above. However, for $k \gtrsim m_D$ the unphysical β modes have $(\mathrm{Re}z)^2 \lesssim 1$. Therefore for large anisotropies and $k \gtrsim m_D$ the effects of the unphysical β modes can have an important impact on the propagator for spacelike modes on the physical Riemann sheet. Additionally, we see that for infinite ξ the Imz of the unphysical β mode vanishes and it then moves to the physical sheet as we will discuss below.

C. Mountains on spirals

As discussed in the previous section we find that, in addition to modes on the physical sheet found in Ref. [7], for anisotropic systems there are also unphysical α and β modes on neighboring Riemann sheets. But why bother about these modes, given that they do not "live" on the physical sheet? To see that there can be an effect on physical quantities, imagine the structure of the complex z plane spanned by the different sheets of the logarithm in the form of a spiral staircase: the physical sheet would correspond to the region covered by the spiral plane from the ground floor to the first floor, while the unphysical sheet where the extra quasiparticle mode lives would correspond to the region first to second floor.

However, since for a range of momenta the unphysical β mode corresponds to an approximately spacelike pole, the propagator has a mountainous dent (singularity) in the spiral plane somewhere from the first to the second floor, with its peak nearer the first floor the larger ξ is. But because the mountain has a finite width, its base can be felt also below the second floor, especially if its peak is near the first floor (see Fig. 6 for a sketch). This is precisely the situation we presented in the previous section. There we showed that in the large-ξ limit that for $k \gtrsim m_D$ the Imz of the unphysical β modes becomes very small and $(\mathrm{Re}z)^2 \lesssim 1$. Therefore, we expect that the unphysical modes on neighboring Riemann sheets do have physical consequences for large anisotropies, since then

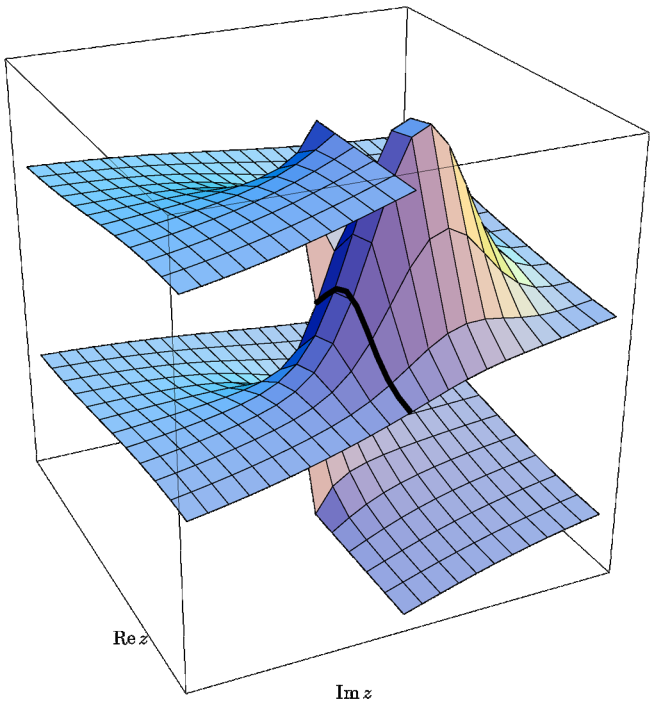

FIG. 6 (color online). Sketch of the complex z plane including the extension of the logarithm to the unphysical sheet. Also shown is how a pole in the unphysical region (mountain) has effects felt on the physical sheet. The black line indicates where the two sheets are joined together.

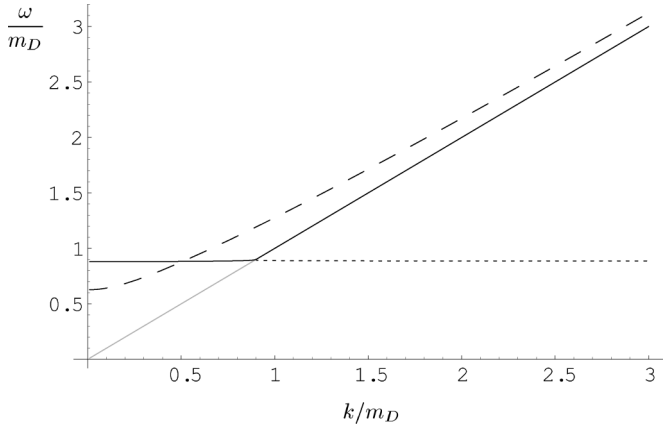

FIG. 7. Dispersion relations for $\theta_n = 0$ and $\xi = 10^4$: the β mode approaches its large-ξ behavior. Again the physical α, physical β, and unphysical β modes are indicated by dashed, solid, and dotted lines, respectively.

their effect can extend down to the physical sheet. In fact, as we will discuss below, in the limit of infinite ξ the pole moves onto the physical sheet itself. Note that the physical effect of any singularities existing on higher Riemann sheets ($|n| > 1$) would be negligible since the effect of these singularities would have to extend through the intermediate sheets prior to getting to the physical sheet, i.e., the base of the mountain would have to extend all the way down to the physical sheet through the spacelike spirals.

D. Towards large ξ

For very large values of ξ, the dispersion relations are shown in Fig. 7. As one can see, the physical β mode now hits the light cone at the point where the unphysical mode becomes spacelike. Indeed, when one takes the limit of $\xi \to \infty$, the β mode simply becomes

$$1 - \frac{\pi}{4}\frac{m_D^2}{\omega^2} = 0, \tag{23}$$

which has the simple real and propagating solution $\omega^2 = \pi m_D^2/4$. For any finite ξ the logarithmic singularity of β in Eq. (11) at the light cone causes the physical β mode to always be timelike; however, the unphysical solution exists for both timelike and spacelike momenta.

IV. SPECIAL CASE II: $\xi \to \infty$

Another special case where one can explicitly calculate the structure functions is when $\xi \to \infty$. In this case it has been found in Ref. [9] that the distribution function becomes

$$\lim_{\xi\to\infty} f_\xi(\mathbf{p}) \to \delta(\hat{\mathbf{p}}\cdot\hat{\mathbf{n}}) \int_{-\infty}^{\infty} dx f_{\rm iso}(p\sqrt{1+x^2}), \tag{24}$$

which corresponds to the extreme anisotropic case considered by Arnold, Lenaghan, and Moore [8]. As a consequence, one can make use of this form by partially integrating Eq. (1) to obtain

$$\Pi^{ij}(K) = 2\pi\alpha_s \int \frac{d^3p}{(2\pi)^3}\frac{f_\xi(\mathbf{p})}{p}\left[\delta^{ij} - \frac{k^i v^j + k^j v^i}{-K\cdot V - i\epsilon} + \frac{(-\omega^2+k^2)v^i v^j}{(-K\cdot V - i\epsilon)^2}\right], \tag{25}$$

and applying the techniques from Ref. [8] to obtain analytic expressions for the structure functions in the large-ξ limit. Using

$$\lim_{\xi\to\infty} 2\pi\alpha_s \int \frac{d^3p}{(2\pi)^3}\frac{f_\xi(\mathbf{p})}{p} = m_D^2\frac{\pi}{4}, \tag{26}$$

the structure functions are obtained using the contractions Eq. (6), giving

$$\alpha = \frac{m_D^2\pi}{4}\left[-\cot^2\theta_n + \frac{z}{\sin^2\theta_n}\left(z \pm \frac{1-z^2}{\sqrt{z+\sin\theta_n}\sqrt{z-\sin\theta_n}}\right)\right], \qquad \beta = \frac{m_D^2\pi}{4}z^2\left[-1 \pm z\frac{z^2+\cos2\theta_n}{(z+\sin\theta_n)^{3/2}(z-\sin\theta_n)^{3/2}}\right],$$
$$\gamma = \frac{m_D^2\pi}{4}\frac{1-z^2}{4\sin^2\theta_n}\left[6 + 2\cos2\theta_n \pm z\frac{3-6z^2-2(1+z^2)\cos2\theta_n - \cos4\theta_n}{(z+\sin\theta_n)^{3/2}(z-\sin\theta_n)^{3/2}}\right],$$
$$\hat{\delta} = \frac{m_D^2\pi}{4}\frac{\cos\theta_n}{\sin^2\theta_n}z\left[z \pm \frac{(1-2z^2)\cos^2\theta_n - (1-z^2)^2}{(z+\sin\theta_n)^{3/2}(z-\sin\theta_n)^{3/2}}\right], \tag{27}$$

where a positive sign above corresponds to the physical sheet and a negative sign corresponds to the unphysical sheet. Note that the light cone singularity at $z^2 = 1$ is not present in these structure functions any longer. In fact, all structure functions turn out to be purely real for $z^2 > \sin^2\theta$ while there is a singularity located at $z^2 = \sin^2\theta$. Below this light cone-like structure, the imaginary parts are nonvanishing.

A. Collective modes

The dispersion relations of the collective modes are once more determined by the zeros of Eq. (13). By conducting a Nyquist analysis similar to the previous section, one finds $N_{\alpha,\rm phys} = 2 + 2\Theta(-\lim_{z\to0}\Delta_A(z))$ and $N_{\Delta_G,\rm phys} = 4 + 2\Theta(\lim_{z\to0}\Delta_G(z))$ for the physical sheet. These modes can be identified as the standard,

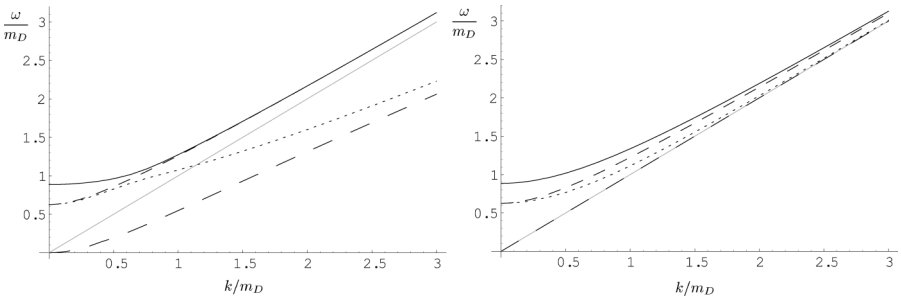

FIG. 8. Dispersion relations for $\xi = \infty$ for (a) $\theta_n = \frac{\pi}{4}$ and (b) $\theta_n = \frac{\pi}{2}$. Shown are the physical α mode (short dashed lines) and the two physical β modes (full and dotted lines) as well as the unphysical β mode (long-dashed lines), respectively. For $\theta_n = 0$, the dispersion relations resemble those of Fig. 7 except that the mode which follows the light cone beyond $k^2 = m_D\pi/4$ in Fig. 7 ceases to exist and the β mode connects continuously across the light cone to the now physical spacelike mode.

propagating modes (one for Δ_α and two for Δ_G together with their negative frequency equivalents) as well as two imaginary modes (one in the UHP and one in LHP) for Δ_α and Δ_G, respectively. The latter again depend only on the sign of the static limit of the propagators, which in the limit of large ξ are functions of the momentum k and the angle θ_n, respectively.[2]

By once again extending the structure functions Eq. (27) to the unphysical sheets in the LHP and UHP (the terms involving square roots simply pick up an overall minus sign) we are also able to count the modes there by repeating the earlier analysis. One finds $N_{\alpha,\mathrm{LHP}} = N_{\alpha,\mathrm{UHP}} = \Theta(\lim_{z\to 0}\Delta_A(z))$ corresponding to a purely imaginary mode, and $N_{\Delta_G,\mathrm{LHP}} = N_{\Delta_G,\mathrm{UHP}} = 2 - \Theta(\lim_{z\to 0}\Delta_G(z))$. The first two of the latter modes are in general complex modes but may—in some restricted region of parameter space—also become purely imaginary solutions; the step function then just encodes the fact that one of the purely imaginary solutions moves to the physical sheet. In Fig. 8 we plot the $\xi = \infty$ dispersion relations for the physical and unphysical collective modes for $\theta_n = \pi/4$ and $\theta_n = \pi/2$.

V. CONCLUSIONS

In this paper we have continued our study of the gluon polarization tensor in an anisotropic system. We extended our previous analysis to unphysical Riemann sheets and showed that for anisotropic distribution functions there are modes (singularities) in the "spacelike region" of the unphysical sheet which become physically relevant for large anisotropies. The chief way that these modes affect the physics is by altering the behavior of the propagator at soft spacelike momenta. The behavior of the propagator in this region determines the rate of energy transfer from soft to hard modes and the sign of this energy transfer may change for anisotropic systems so that there is instead a transfer of energy from hard to soft modes [16]. Whether or not the presence of the modes on the unphysical Riemann sheets are responsible for this "anti-Landau damping" is investigated in a separate paper [17] in which we compute heavy fermion energy loss in a quark-gluon plasma along the lines of Ref. [18] in which we calculated the same in an anisotropic QED plasma.

In addition to these unphysical β modes we found that for anisotropic distributions the unphysical α modes are different than in the isotropic case. In the isotropic case, there are two unphysical α modes with one being in the upper half plane of the $n = 1$ unphysical sheet and one in the lower half plane of the $n = -1$ unphysical sheet. We showed that for finite ξ and small momentum these isotropic unphysical modes move onto the physical sheet and become the unstable modes already discussed in Ref. [7]. Additionally, for finite anisotropy there are two additional unphysical α modes, again, with one being in the upper half plane and one in the lower half plane. These modes would, in principle, determine the dynamic screening of the magnetic gluon interaction at small momentum; however, the instabilities in this region will dominate the physics so it is not entirely obvious how important these additional unphysical α modes are.

Note that in this paper we have considered only the gluon polarization tensor which is itself not an observable. In order to say anything quantitative about the impact of these types of modes we must compute an actual observable. In general, any observable which is sensitive to spacelike momenta will be affected by these types of unphysical modes; however, the quantitative impact will vary depending on the observable in question. In a forthcoming paper [17], we compute one such observable, the collisional energy loss of a heavy quark propagating in an anisotropic quark-gluon plasma. In that paper we show that for $\alpha_s = 0.3$ and a 20 GeV bottom quark that the deviations from the isotropic result are on the order of 10% for $\xi = 1$ and of the order of 20% for $\xi \geq 10$. When translated into the difference between longitudinal and transverse energy loss this results in a 10% difference at $\xi = 1$, a 30% difference at $\xi = 10$, and a 50% difference at $\xi = \infty$. More importantly, however,

[2]See Ref. [9] for a discussion of the static limit of Eq. (27).

we found that for small velocities the sign of the energy loss becomes *negative* representing energy gain instead of loss whenever $\xi > 0$. The origin of this negative energy loss is explicitly identified as being an unphysical type-1 α mode. In addition the negative energy loss is shown to vanish in the isotropic limit giving a positive definite result for this quantity for all velocities.

In closing we would like to point out that although the finite-ξ analysis presented here was performed only for $\theta_n = 0$ there are generally relevant unphysical α and β modes for all angles of propagation. The analysis proceeds exactly as discussed here but the details (number of modes, etc.) change here and there. Additionally, the results presented here are also applicable to anisotropic ultrarelativistic QED plasmas.

ACKNOWLEDGMENTS

The authors would like to thank A. Rebhan for very useful discussions and feedback. M. S. was supported by the Austrian Science Fund Project No. M790-N08.

[1] M. Gyulassy and L. McLerran, nucl-th/0405013; M. Gyulassy, nucl-th/0403032; U.W. Heinz and P.F. Kolb, hep-ph/0204061; U.W. Heinz, Nucl. Phys. **A721**, 30 (2003).
[2] St. Mrówczyński, Phys. Rev. C **49**, 2191 (1994).
[3] St. Mrówczyński, Phys. Lett. B **393**, 26 (1997).
[4] St. Mrówczyński and M.H. Thoma, Phys. Rev. D **62**, 036011 (2000).
[5] M.C. Birse, C.W. Kao, and G.C. Nayak, Phys. Lett. B **570**, 171 (2003).
[6] J. Randrup and St. Mrówczyński, Phys. Rev. C **68**, 034909 (2003).
[7] P. Romatschke and M. Strickland, Phys. Rev. D **68**, 036004 (2003).
[8] P. Arnold, J. Lenaghan, and G.D. Moore, J. High Energy Phys. 08 (2003) 002.
[9] P. Romatschke, Ph.D. thesis, Vienna Technical University, hep-ph/0312152.
[10] St. Mrówczyński, A. Rebhan, and M. Strickland, Phys. Rev. D **70**, 025004 (2004).
[11] E.S. Weibel, Phys. Rev. Lett. **2**, 83 (1959).
[12] I.B. Bernstein, J.M. Greene, and M.D. Kruskal, Phys. Rev. **108**, 546 (1957).
[13] R.L. Berger and R.C. Davidson, Phys. Fluids **15**, 2327 (1972).
[14] R.C. Davidson, D.A. Hammer, I. Haber, and C.E. Wagner, Phys. Fluids **15**, 317 (1972).
[15] T.-Y.B. Yang, Y. Gallant, J. Arons, and A.B. Langdon, Phys. Fluids B **5**, 3369 (1994); T.-Y.B. Yang, J. Arons, and A.B. Langdon, Phys. Plasmas **1**, 3059 (1994).
[16] E.M. Lifshitz and L.P. Pitaevskii, *Physical Kinetics* (Pergamon Press, Oxford, 1981).
[17] P. Romatschke and M. Strickland, hep-ph/0408275.
[18] P. Romatschke and M. Strickland, Phys. Rev. D **69**, 065005 (2004).